Article

# Saturation of the filament density of ultrashort intense laser pulses in air

HENIN, Stefano, *et al*.

**Abstract**

We experimentally and numerically characterize multiple filamentation of laser pulses with incident intensities of a few TW/cm2. Propagating 100 TW laser pulses over 42 m in air, we observe a new propagation regime where the filament density saturates. As also evidenced by numerical simulations in the same intensity range, the total number of filaments is governed by geometric constraints and mutual interactions among filaments rather than by the available power in the beam.

Reference

HENIN, Stefano, *et al*. Saturation of the filament density of ultrashort intense laser pulses in air. *Applied physics. B, Lasers and optics*, 2010, vol. 100, no. 1, p. 77-84

DOI : 10.1007/s00340-010-3941-x

Appl Phys B (2010) 100: 77–84
DOI 10.1007/s00340-010-3941-x

**Applied Physics B**
**Lasers and Optics**

# Saturation of the filament density of ultrashort intense laser pulses in air

**S. Henin · Y. Petit · J. Kasparian · J.-P. Wolf · A. Jochmann · S.D. Kraft · S. Bock · U. Schramm · R. Sauerbrey · W.M. Nakaema · K. Stelmaszczyk · P. Rohwetter · L. Wöste · C.-L. Soulez · S. Mauger · L. Bergé · S. Skupin**

Received: 11 February 2010 / Published online: 16 March 2010


**Abstract** We experimentally and numerically characterize multiple filamentation of laser pulses with incident intensities of a few TW/cm$^2$. Propagating 100 TW laser pulses over 42 m in air, we observe a new propagation regime where the filament density saturates. As also evidenced by numerical simulations in the same intensity range, the total number of filaments is governed by geometric constraints and mutual interactions among filaments rather than by the available power in the beam.

## 1 Introduction

The propagation of ultrashort intense laser pulses in air or other transparent media is characterized by filamentation [1–5], a self-sustained propagation regime where a dynamical balance is established between Kerr-lens self-focusing and defocussing by further nonlinear processes like interaction with plasma generated at the nonlinear focus or other higher-order saturation effects [6]. Filamentation is now well characterized from the milli-Joule to the sub-Joule levels, corresponding to powers from the GW up to the TW for pulse durations in the fs range. Recently, we demonstrated that filamentation still occurs at the multi-J level [7], displaying similar physics as at lower energies. However, this experiment was conducted with relatively long pulses between 520 fs and 65 ps. Moreover, the beam was emitted vertically, so that filaments were observed indirectly by imaging or LIDAR (Light Detection and Ranging) from the ground. Therefore, a direct comparison of multi-TW pulse dynamics with the experimentally reported results at much lower powers and shorter pulse durations (30–200 fs) was not straightforward.

A prominent property classically attributed to filamentation is the linear dependency of the filament number with the input power. As early as 1973, Campillo et al. [8] theoretically predicted from the cubic Schrödinger equation that self-focusing cells should each contain a number of critical powers, $P_{cr}$, depending on their shape, with a minimum of $6.7P_{cr}$ in the case of square cells. In the context of self-channeling of femtosecond filaments, several experimental data collected from different laser systems confirmed a linear dependence of the filament number with power, with one filament per $\sim 5P_{cr}$ ($P_{cr} \approx 4$ GW in air at 800 nm). Such value was observed close to the filamentation threshold [9–11], in the multiple-filamentation regime of TW-class lasers [12], as well as in the case of multi-TW, multi-Joule experiments (26 J, 32 TW) [7].

In this work, we investigate the horizontal propagation of a 3 J, 100 TW (30 fs) laser pulse over 42 m in air. We char-

S. Henin · Y. Petit · J. Kasparian (✉) · J.-P. Wolf
Teramobile, GAP, Université de Genève, 20 rue de l'Ecole de Médecine, 1211 Genève 4, Switzerland
e-mail: jerome.kasparian@unige.ch

A. Jochmann · S.D. Kraft · S. Bock · U. Schramm · R. Sauerbrey
Forschungszentrum Dresden-Rossendorf, Bautzner Landstraße 400, 01328 Dresden, Germany

W.M. Nakaema · K. Stelmaszczyk · P. Rohwetter · L. Wöste
Teramobile, Institut für Experimentalphysik, Freie Universität Berlin, Arnimallee 14, 14195 Berlin, Germany

C.-L. Soulez · S. Mauger · L. Bergé
CEA, DAM, DIF, 91297 Arpajon, France

S. Skupin
Max Planck Institute for the Physics of Complex Systems, 01187 Dresden, Germany

S. Skupin
Institute of Condensed Matter Theory and Optics, Friedrich Schiller University, 07742 Jena, Germany

acterize the density of the high-intensity filaments, which substantially deviates from the above-recalled linear dependency. This deviation results from the saturation of the filament number per unit surface of the transverse beam profile, based on the typical cross-section of the photon bath surrounding the filament cores along their self-guiding. Dimensions of this cross-section put an upper limit on the local filament density, which becomes almost independent of the input power along the self-guiding range. While our finding challenges the previously established linearity rule, it provides new evidence that both the filament occupation constraints inside photon baths and their mutual interaction are key ingredients of the multifilamentation dynamics. Three-dimensional numerical simulations confirm these features by reproducing the major experimental patterns at comparable incident intensities over smaller beam scales.

## 2 Material and methods

Experiments were performed using the Ti:Sa chirped pulse amplification chain at Forschungszentrum Dresden-Rossendorf. The laser provided up to 3 J, 100 TW pulses of 30 fs duration, at a repetition rate of 10 Hz and central wavelength of 800 nm. The pulse energy was adjusted by rotating a half-waveplate associated with a polarizer before the grating compressor. The beam was transported in a vacuum tube to the experimental hall, where it was launched, collimated (i.e. as a parallel beam) with a diameter of $\sim$10 cm, through a 6 mm thick fused silica window, into 42 m of free propagation in air. The dispersion in the window was precompensated by adequately adjusting the grating compressor of the laser system.

The multiple filamentation of the beam was characterized by both single-shot burns on photosensitive paper (Kodak Linagraph 1895, see Fig. 1), and single-shot still photographs on an optically neutral screen, recorded by a CCD camera equipped with density filters. Each filament in the beam profile was then individually identified on the images or burns, as a bright or a black spot, respectively, and located by its transverse coordinates relative to the centre of the beam. The same process, performed on either of the red, green or blue layers of the CCD camera or the burn images, yielded consistent filament numbers, with typically 10% deviations. Based on this filament identification, we computed the local filament density at any location across the laser beam.

Densitometry measurements on the red layer of the CCD camera images provided fluence profiles of the beam, which were calibrated by integrating this profile over the transverse plane at the considered propagation distance $z$ and normalizing through the input pulse energy, neglecting the losses along propagation. This method mainly focuses on the photon bath and discards the most intense part of the filaments, which occupy a small fraction of the profile and whose fluence is truncated by the dynamics of the detector. The fluence profile is converted into intensity by dividing all flu-

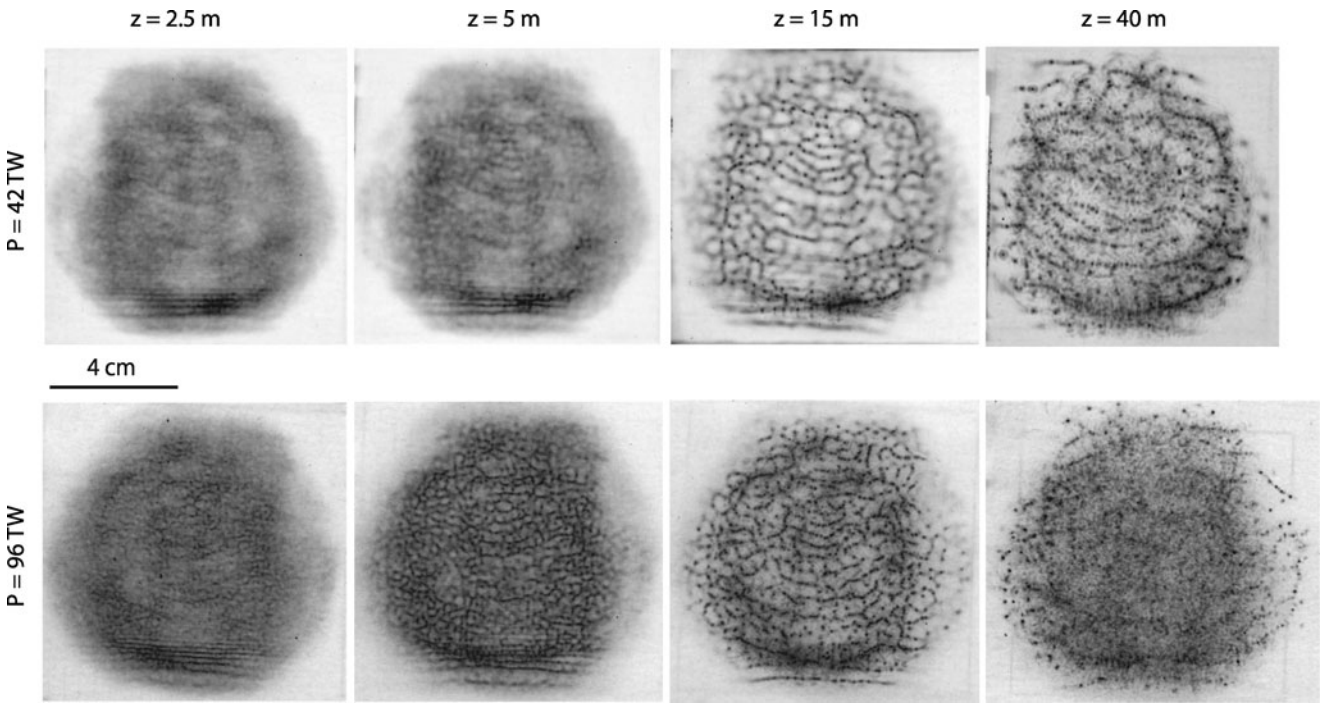


**Fig. 1** Beam profiles on burn paper of multi-TW, 30 fs pulses propagating in air, as a function of the incident power and propagation distance. Most filaments appear on lines along which filaments are spaced by a few mm

ence values by the pulse duration, which is assumed to be close to the initial one, since the photon bath is barely affected by plasma temporal distortions.

To get more insight into the mechanism leading to the saturation of the filament density, we performed a spatially resolved analysis of the measured intensity profiles. We sampled the beam profile into 187 square elementary surfaces of 6.6 mm × 6.6 mm. In each elementary surface at location $\mathbf{r}$, we counted the filament number, which, divided by the elementary surface provided the local density of filaments $N(\mathbf{r})$. Moreover, the intensity profile from the densitometry, numerically averaged over the elementary surface, provided the local photon bath intensity $I_{\text{bath}}(\mathbf{r})$. We next compute the ratio $p(\mathbf{r}) = I_{\text{bath}}(\mathbf{r})/N(\mathbf{r})$ in each elementary surface. This ratio corresponds to the power per filament in the considered surface, around the considered transverse position $\mathbf{r}$ in the beam. Owing to the transverse dimension of the beam and the fact that interactions between self-focusing cells are local, we consider the 187 elementary surfaces as almost independent. Sorting the elementary surfaces according to their intensity and averaging the values of $N(\mathbf{r})$ for each value of $I_{\text{bath}}$ yield the average value $N(I_{\text{bath}})$ and thereby the mean value of $p$ for any $I_{\text{bath}}$: $p(I_{\text{bath}})$, which will be plotted in Fig. 4.

To understand the mechanism of filament saturation along the self-guiding stage, we also integrated the standard propagation model (so-called Nonlinear Envelope Equation [3]) in complete space and time resolved $(3+1)$-dimensional geometry. This model governs the laser electric field envelope $E$ with intensity $I = |E|^2$ and a source equation describes plasma generation. The propagation equations take into account chromatic dispersion of air, space-time focusing and self-steepening terms, and nonlinear (cubic) polarization with Kerr index $n_2 = 2.5 \times 10^{-19}$ cm$^2$/W ($P_{\text{cr}} = 4$ GW) including an instantaneous part and a Raman-delayed contribution in ratio 1/2. This choice of parameters particularly suits ultrashort infrared pulses with durations $\leq 50$ fs [13, 14], undergoing plasma coupling and multiphoton absorption losses. The source equation governing the free electron density $\rho$ includes a photo-ionization rate approached by $W(I) = \sigma_K I^K$ with cross-section $\sigma_K = 2.9 \times 10^{-99}$ s$^{-1}$ cm$^{2K}$/W$^K$ ($K = 8$ is the minimum photon number requested for ionization of $O_2$ molecules at the laser wavelength $\lambda_0 = 800$ nm), together with avalanche ionization depending on an electron collision time of 350 fs. Electron recombination is neglected over the short time scale of the pulses.

## 3 Results and discussion

Figure 1 displays typical multifilamentation patterns at propagation distances up to $z = 40$ m. The filamentary cells are organized in quasi-parallel strings mutually separated by a few mm. In each string, the filaments, identified as the most spiky structures, are separated by 1–2 mm from each other. These strings can be composed of optical cells with lower fluence, which are therefore not identified as intense filaments. The total number of filaments in the beam profile is displayed in Fig. 2 as a function of the propagation distance and the incident power. Up to 700 intense filaments are generated in the beam profile. Although this number may appear large in absolute value, it remains modest compared with the power involved. At 800 nm, an incident power close to 100 TW typically corresponds to $25{,}000 P_{\text{cr}}$, which would be expected to generate up to 5000 filaments at the rate of $5P_{\text{cr}}$ per filament. Actually, the filament number appears to be divided by a factor of almost 10 at all investigated input energies. From Figs. 1 and 2, we can see that the total number of filaments remains in the same order of magnitude over several meters. The focal spot produces a universal pattern involving a reduced number of ordered hot spots.

Figure 3 displays statistics about the local filament density $N(\mathbf{r})$ over all elementary grid surfaces of 6.6 mm × 6.6 mm across the beam profile of the 96 TW pulse after 15 m of propagation. Consistent with the strong saturation of the filament number in the overall beam, the local filament density is limited to $N_{\text{fil}} \sim 10$ filaments/cm$^2$, a value

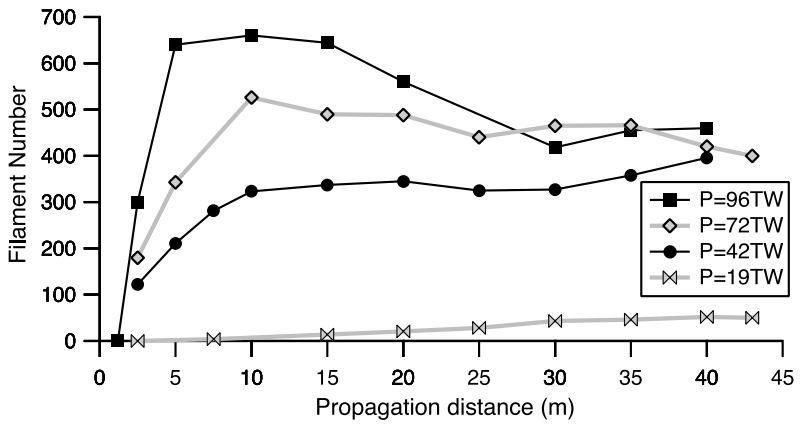


**Fig. 2** Filament number as a function of the propagation distance and energy

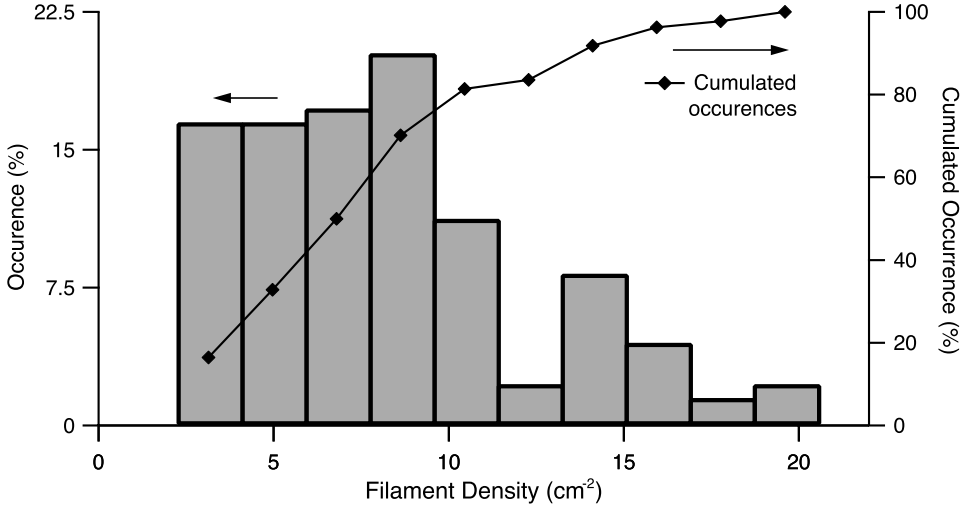


**Fig. 3** Occurrence distribution of the local filament density at the propagation distance $z = 15$ m for the 96 TW pulse

exceeded in only 20% of the elementary surfaces. This density corresponds to a typical distance of ∼3 mm between the nearest filaments. For comparison, a photon bath intensity of $10^{13}$ W/cm$^2$ would yield a density of ∼500 filaments/cm$^2$ at the classical rate of $5P_{cr}$/filament. This reduced filament density was observed all along the available propagation distances, up to 42 m, as well as when reducing the incident pulse energy or chirping the incident pulses.

Due to the strong inhomogeneity of the background intensity profile across the beam, $I_{bath}$ spans over a range of more than one order of magnitude, providing the opportunity to investigate the filament density $N$ as a function of intensity over this range. Figure 4 displays this information, showing the ratio $p(I_{bath}) = I_{bath}/N(I_{bath})$ as defined in the previous section and expressed in units of $P_{cr}$. This presentation facilitates the estimation of the power required to generate a filament in given conditions. For example, a constant power of $5P_{cr}$/filament, observed at low incident intensities, would result in the horizontal dotted line displayed in Fig. 4. Clearly, experimental data substantially deviate from this trend as soon as $I_{bath}$ exceeds a few $10^{11}$ W/cm$^2$, showing that the saturation of the filament density does not only occur in the overall beam, but also in the local dynamics of the filamentary cells. Data reported from the literature [7, 11, 12, 15] are also plotted for reference: They fit well with our present data and show that current high-power laser systems can reach this saturation regime (see the "Helvetera" data), which had however not been identified so far.

It is well-known from both theory [16, 17] and experiments [18, 19] that isolated filaments form, besides their inner core, a surrounding photon bath with transverse dimensions of several hundreds of μm. Consequently, filaments in principle require a minimum surface of several mm$^2$ to develop. This cross-section corresponds to millimeter-range spacing between filaments, under which neighboring optical cells weakly interact. The mutual attraction of filaments located a few mm apart has already been well described [20–25]. In our experiments, since we did not focus the beam, neighboring filaments can be expected to emerge in phase since they are issued from the same beam, so that interactions will be mainly attractive. In fact, we expect that in the merging process, robust filaments conveying the highest intensity will "absorb" the less intense optical cells. Therefore, underlying the saturation mechanism that limits the filament density, the interaction between filaments, initiated by their overlapping photon baths, can result in the merging of the "in excess" filaments. This merging mechanism here involves the Kerr self-focusing effect, altered by plasma generation and related losses, acting all together on interacting cells which occupy a few mm$^2$ in the beam profile at distances where the filamentation is most active. This process can be compared to that observed in the case of two beams crossing in glass, where the interferences in the photon bath reduce the available energy for filamentation and therefore decrease the filament number [26].

Thus, filaments do not only require a minimal power of $5P_{cr}$ to be initiated, but also a minimum surface to develop and survive with their own photon bath. This minimum surface can be determined as the counterpart of the upper limit of the filament density of $N_{fil} \sim 10$ cm$^{-2}$ observed in the data of Fig. 3. On this basis, we can express the fact that the filament density $N(\mathbf{r})$ around the position $\mathbf{r}$ (e.g., the center of one elementary surface inside the beam) is limited by both of these constraints. An approximate description can therefore be provided by the evaluation:

$$N(\mathbf{r}) = \min\left[I_{bath}(\mathbf{r})/5P_{cr};\, N_{fil}\right]. \quad (1)$$

Accordingly, the number of critical powers required to generate a filament expresses in terms of the input beam power $P_{in}$ as

$$I_{bath}(\mathbf{r})/\left[N(\mathbf{r})P_{cr}\right] = \max\left[5;\, I_{bath}(\mathbf{r})/(N_{fil}P_{cr})\right]. \quad (2)$$

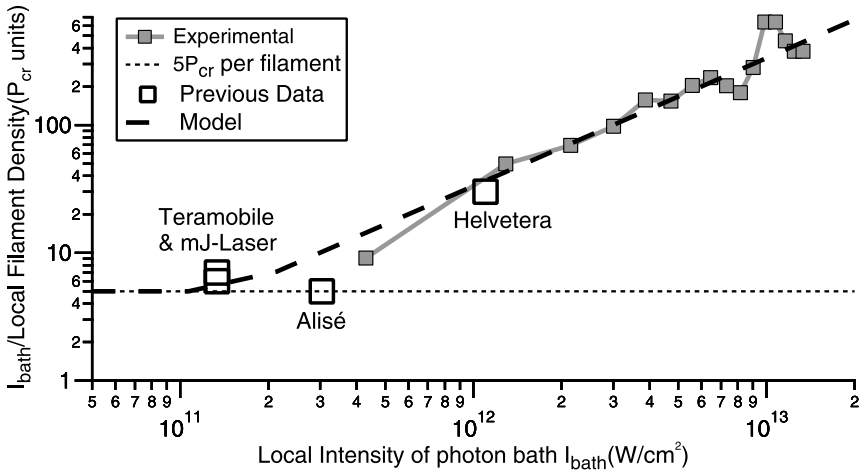


**Fig. 4** Experimental data and model (2) of the local filament density as a function of the local photon bath intensity $I_{\text{bath}}$ at $z = 15$ m for the 96 TW pulse. Previously published data in different experimental conditions are displayed for reference: Multi-TW, 100 fs pulses (Teramobile laser) [12], multijoule, picosecond pulses (Alisé laser) [7], a TW, 30 fs laser (Helvetera system) [15], and a mJ, 120 fs laser (single filamentation) [11]

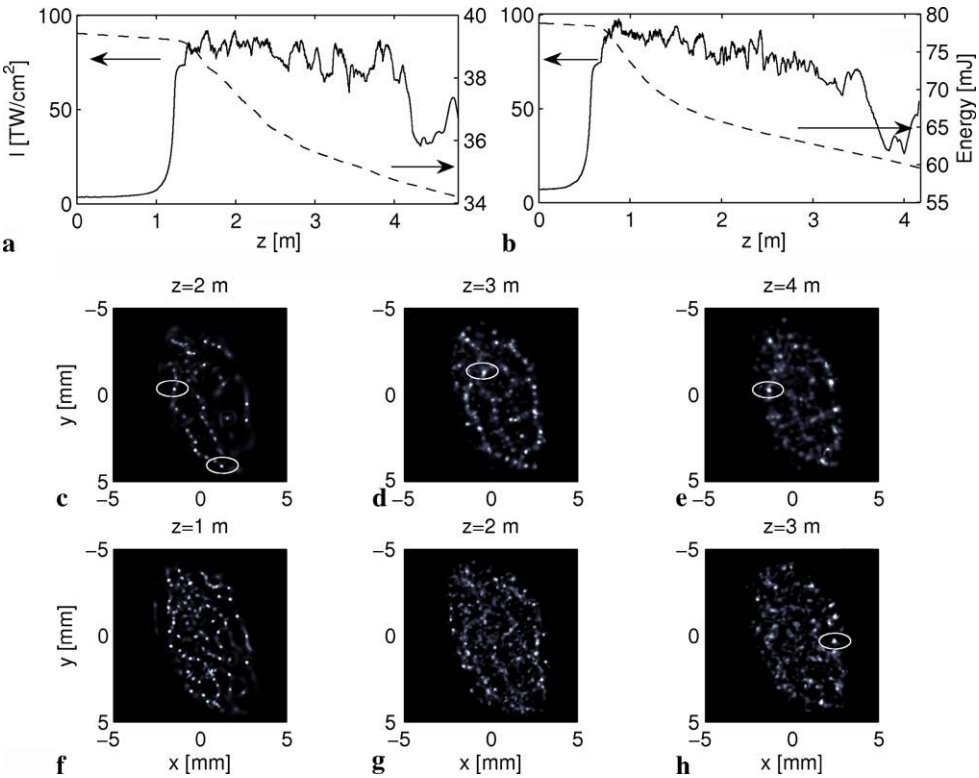


**Fig. 5** Peak intensities (*solid curves*, *units on the left-hand side axis*) and energy losses (*dashed curves*, *units on the right-hand side axis*) for the beams with (**a**) $300P_{\text{cr}}$ and (**b**) $600P_{\text{cr}}$ computed numerically using $1/e^2$ beam waist of 5 mm in air. (**c**, **d**, **e**) and (**f**, **g**, **h**) show their respective fluence distributions in the $(x, y)$ plane. White ellipses exemplify intense filaments with highest fluence

The low-intensity case of (1) and (2) corresponds to standard power regimes, while the high-intensity case is for the first time examined in this work. Figure 4 compares the outcome of this simple model with the experimental data. Despite the simplicity of the model, the agreement is excellent, showing the validity of the simple model proposed to predict the filament density at high intensities.

Our measurements therefore define a new filamentation regime, where the filament number density saturates at high input optical powers. This result apparently contradicts previous observations showing longer filamentation ranges and higher $N_2$ fluorescence when the beam diameter is reduced [27–29]. However, these works did not directly measure the number of filaments, but rather the $N_2$ fluorescence emitted backwards in LIDAR configuration. In fact, closely packed filaments may here be issued from the merging of several filament germs and be longer and/or more intense, yielding a stronger signal integrated along the filamenting range.

The saturation of the filament density is also well evidenced by $(3 + 1)$-dimensional numerical simulations, whose results are summarized in Figs. 5 and 6. Due to the limitations of current computer capabilities, we could not simulate the $\sim$100 cm$^2$ of the beam shown in Fig. 1 with adequate transverse resolution. Rather, we considered a smaller beam, with a long-axis beam waist of 5 mm at $1/e^2$, comparable to the size of the elementary surfaces used in the

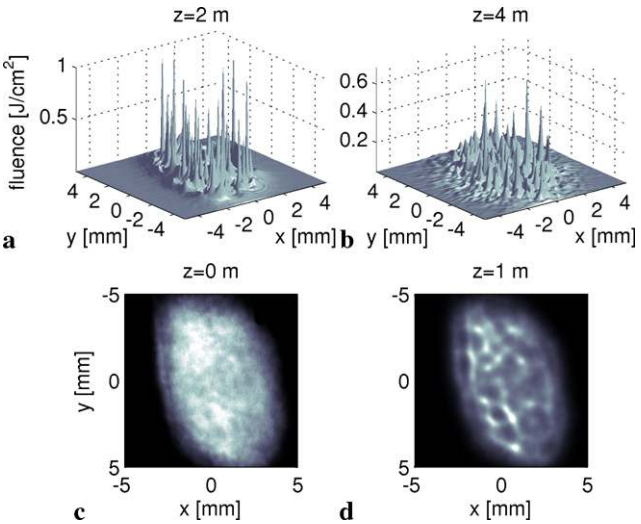


**Fig. 6** Surface plots of the transverse fluence profiles of the $300P_{cr}$ beam at (**a**) $z = 2$ m and (**b**) $z = 4$ m. Image cuts of the fluence profiles of the $300P_{cr}$ beam at (**a**) $z = 0$ and (**b**) $z = 1$ m

analysis of the experimental data. Since this size is close to the focal spots examined in [30], we used a fluence profile previously simulated in Fig. 9 of that work and recalled in Fig. 6(c). In order to investigate the saturation of the filament number at high intensities comparable to those of the experiments, this profile was scaled to a power of $P_{in} = 300P_{cr}$ or $P_{in} = 600P_{cr}$. These values correspond to a peak intensity of 3.5 and 7 TW/cm$^2$, respectively, comparable to that of the experimental measurements. We therefore cannot expect to reproduce systematically the multifilamentation pattern of Fig. 1, but rather to test the evolution of the filament number along the self-channeling range. Simulations ran over 256 processors and guaranteed fine resolution in both space ($\Delta x = \Delta y = 1$ μm) and time ($\Delta t = 0.6$ fs), with an adaptive step $\Delta z$ along the propagation axis.

Figure 5(a) and (b) show the peak pulse intensities (solid curves) and energy losses owing to plasma generation (dashed curves) along the 4 m long propagation range, followed by pulse relaxation. The plasma density forms an almost flat plateau around the peak value $\rho_{max} = 5 \times 10^{16}$ cm$^{-3}$ (not shown). Importantly, the energy losses become more pronounced at higher incident peak powers: Over the first three meters after the nonlinear focus, the relative energy loss due to plasma generation is about 10% for the $300P_{cr}$ pulses, whereas it reaches 20% for 600 $P_{cr}$. Furthermore, Fig. 5(c, d, e) and (f, g, h) display the fluence patterns at distances beyond the nonlinear focus. Fluence is here truncated at the maximum level of 1 J/cm$^2$, in order to discriminate better between optical structures with high and low local intensities.

Similarly to the experimental observation, filaments emerge near to the nonlinear focus along quasi-parallel lines within the profile. These lines stem from the initial beam inhomogeneities, from which small-scaled filaments emerge (see the "optical pillars" scenario in Ref. [30]). As expected, more cells appear in the fluence pattern with double input power. Near the nonlinear focus, we count around 46 and 116 cells at $z = 2$ and 1 m for the 300 and $600P_{cr}$ beams, respectively. These filament numbers are compatible with the 60 and 120 filaments predicted by the classical estimation of $5P_{cr}$ per filament. However, in the beam with $300P_{cr}$, only 20 of them (the brightest spots) are capable to exceed a fluence of 0.5 J/cm$^2$, as detailed in Fig. 6(a). A couple of meters beyond, due to energy exchanges and active plasma defocussing [22], the weak cells are absorbed by the photon bath surrounding the strongest filaments, among which 8 can still reach the same fluence level [Fig. 6(b)] within the beam surface of ∼0.5 cm$^2$. With double power, more intense filaments are created near focus, but their number relaxes to quite similar values, i.e., around 9–10 filaments two meters after the nonlinear focus. Such process clearly illustrates the saturation of the filament density at very high incident intensities. Note the strong evacuation of energy in the beam with higher power, so that both fluence patterns become more resembling at $z = 4$ m. Their geometric structure emphasizes more clearly the quasi-parallel lines of filaments, mutually spaced by ≈2–3 mm from each other. Scaled to $25{,}000P_{cr}$, this estimation should correspond to ∼400–1600 filaments, in reasonable agreement with the experiments (Fig. 2). Furthermore, a numerical evaluation of the $300P_{cr}$ beam background intensity, $I_{bath} \approx 3.2$ TW/cm$^2$, that supports the filamentary spikes with mean density of 16–20 intense filaments/cm$^2$ beyond the nonlinear focus, yields between 40 and $50P_{cr}$, which holds the comparison with the curve inferred from (2) and plotted in Fig. 4.

Considering the different transverse scales of the beams, we suggest that a comparison with the experimental data requires to scale the propagation distance according to the nonlinear focal lengths, which we estimate to be approximately 15 and 1.5 m in the case of the experiments and numerical simulations, respectively. Figure 6(c) and (d) illustrate the transverse fluence patterns in the early Kerr stage of the $300P_{cr}$ beam. Before the nonlinear focus, Kerr-induced modulational instability breaks up the focal spot into primary cells mutually separated by the optimum transverse wavelength $\lambda_{opt} = w_0\lambda_0(\pi/n_2P_{in})^{1/2} \approx 1.3$ mm [7, 11] along the highest intensity zones of the input beam. So, the initial beam defects do condition the location of the mm-spaced strings which will further be amplified.

These numerical results confirm the experimental findings, showing that over long propagation distances, the number of atmospheric high-intensity filaments becomes independent of the initial pulse intensity and power. Light spots thus tend to exhibit similar distance of mutual separation in the mm range. Energy losses, although relatively small, help the filaments to be distributed into an "equilibrium"

pattern involving a smaller density of hot spots than in classical expectations. Small-scaled filaments are embedded inside mm-spaced strings, which are primarily designed by the fluctuations of the initial beam profile. Hence, filamentary ultrashort broad pulses tend to self-organize into a robust macroscopic ordered structure, which departs to some extent from the optically-turbulent light guide scenario proposed in Ref. [31].

Going back to the fusion mechanism recalled in the previous section, two filaments modeled as Gaussians of waist $w_{\rm fil} \approx 150$ μm are distinguishable if their initial separation distance $\delta$ exceeds $2^{1/2} w_{\rm fil}$. In purely Kerr media, they are expected to coalesce if their individual power is larger than $P_{\rm cr}/4$ but remains below critical [20]. In the presence of nonlinear saturation (plasma defocussing), however, filaments with an initial distance $\delta \leq 10^{1/2} w_{\rm fil}$ can merge up to a power $P_{\rm fil} \leq 1.35 P_{\rm cr}$ [30]. In this case, nonlinear losses relax these constraints as the filaments reach lower, near-critical powers allowing merging even from larger separation distances. Multiphoton absorption thus promotes the mutual coalescence of filaments from separation distances larger than $10^{1/2} w_{\rm fil} \approx 0.5$ mm, i.e., over the mm scale. These arguments indicate that, at the very best, only one filament can be expected to occupy an area of about 1 mm$^2$ inside the focal spot in plasma regime, which thereby justifies the experimental and numerical observations.

## 4 Conclusion

We have investigated experimentally and numerically the multiple filamentation of high-intensity ultrashort laser pulses over 42 m in air. The filament density substantially deviates from usual linear variation with peak power, exhibiting a saturation of the filament number density across the beam profile. This saturation can be understood by considering the interaction of neighboring filaments, resulting in their mutual attraction when they are closer than a few mm from their nearest neighbors. Three-dimensional numerical simulations confirm this saturation mechanism and specify two characteristic processes in the filament dynamics: First, quasi-parallel strings of filaments are preconditioned by the initial modulations at the top of the incident beam. Second, along the propagation range promoting plasma generation and multiabsorption losses, filamentary cells bearing the highest fluences become mutually separated by mm-range distances, above which their possible fusion ceases.

**Acknowledgements** This work was granted access to the HPC resources of CCRT under the allocation 2009-x2009106003 made by GENCI (Grand Equipement National de Calcul Intensif). We acknowledge financial support from the Swiss National Science Foundation (FNS, Grants 200021-116198 and 200021-125315).

## References

1. J. Kasparian, M. Rodriguez, G. Méjean, J. Yu, E. Salmon, H. Wille, R. Bourayou, S. Frey, Y.-B. André, A. Mysyrowicz, R. Sauerbrey, J.-P. Wolf, L. Wöste, Science **301**, 61 (2003)
2. A. Couairon, A. Mysyrowicz, Phys. Rep. **44**, 47 (2007)
3. L. Bergé, S. Skupin, R. Nuter, J. Kasparian, J.-P. Wolf, Rep. Prog. Phys. **70**, 1633 (2007)
4. J. Kasparian, J.-P. Wolf, Opt. Express **16**, 466 (2008)
5. S.L. Chin, S.A. Hosseini, W. Liu, Q. Luo, F. Théberge, N. Aközbek, A. Becker, V.P. Kandidov, O.G. Kosareva, H. Schroeder, Can. J. Phys. **83**, 863 (2005)
6. P. Béjot, J. Kasparian, S. Henin, V. Loriot, T. Vieillard, E. Hertz, O. Faucher, B. Lavorel, J.-P. Wolf, Phys. Rev. Lett. **104**, 103903 (2010)
7. P. Béjot, L. Bonacina, J. Extermann, M. Moret, J.P. Wolf, R. Ackermann, N. Lascoux, R. Salamé, E. Salmon, J. Kasparian, L. Bergé, S. Champeaux, C. Guet, N. Blanchot, O. Bonville, A. Boscheron, P. Canal, M. Castaldi, O. Hartmann, C. Lepage, L. Marmande, E. Mazataud, G. Mennerat, L. Patissou, V. Prevot, D. Raffestin, J. Ribolzi, Appl. Phys. Lett. **90**, 151106 (2007)
8. A.J. Campillo, S.L. Shapiro, B.R. Suydam, Appl. Phys. Lett. **23**, 628 (1973)
9. A.C. Bernstein, J.-C. Diels, T.S. Luk, T.R. Nelson, A. McPherson, S.M. Cameron, Opt. Lett. **28**, 2354 (2003)
10. W. Liu, S.L. Chin, Opt. Express **13**, 5750 (2005)
11. R. Salamé, N. Lascoux, E. Salmon, J. Kasparian, J.P. Wolf, Appl. Phys. Lett. **91**, 171106 (2007)
12. G. Méjean, J. Kasparian, J. Yu, E. Salmon, S. Frey, J.-P. Wolf, S. Skupin, A. Vinçotte, R. Nuter, S. Champeaux, L. Bergé, Phys. Rev. E **72**, 026611 (2005)
13. A. Couairon, S. Tzortzakis, L. Bergé, M. Franco, B. Prade, A. Mysyrowicz, J. Opt. Soc. Am. B **19**, 1117 (2002)
14. S. Champeaux, L. Bergé, D. Gordon, A. Ting, J. Peñano, P. Sprangle, Phys. Rev. E **77**, 036406 (2008)
15. S. Henin, Y. Petit, D. Kiselev, J. Kasparian, J.-P. Wolf, Appl. Phys. Lett. **95**, 091107 (2009)
16. S. Skupin, L. Bergé, U. Peschel, F. Luderer, Phys. Rev. Lett. **93**, 023901 (2004)
17. M. Kolesik, J.V. Moloney, Opt. Lett. **29**, 590 (2004)
18. F. Courvoisier, V. Boutou, J. Kasparian, E. Salmon, G. Méjean, J. Yu, J.-P. Wolf, Appl. Phys. Lett. **83**, 213 (2003)
19. W. Liu, F. Théberge, E. Arévalo, J.-F. Gravel, A. Becker, S.L. Chin, Opt. Lett. **30**, 2602 (2005)
20. L. Bergé, M.R. Schmidt, J. Juul Rasmussen, P.L. Christiansen, K.O. Rasmussen, J. Opt. Soc. Am. B **14**, 2550 (1997)
21. L. Bergé, C. Gouédard, J. Schjodt-Eriksen, H. Ward, Physica D (Amsterdam) **176**, 181 (2003)
22. S.A. Hosseini, Q. Luo, B. Ferland, W. Liu, S.L. Chin, O.G. Kosareva, N.A. Panov, N. Aközbek, V.P. Kandidov, Phys. Rev. A **70**, 033802 (2004)
23. C. Ren, R.G. Hemker, R.A. Fonseca, B.J. Duda, W.B. Mori, Phys. Rev. Lett. **85**, 2124 (2000)
24. Y.-Y. Ma, X. Lu, T.-T. Xi, Q.-H. Gong, J. Zhang, Appl. Phys. B **93**, 463 (2008)
25. E. D'Asaro, S. Heidari-Bateni, A. Pasquazi, G. Assanto, J. Gonzalo, J. Solis, C.N. Afonso, Opt. Express **17**, 17150 (2009)
26. K. Stelmaszczyk, P. Rohwetter, Y. Petit, M. Fechner, J. Kasparian, J.-P. Wolf, L. Wöste, Phys. Rev. A **79**, 053856 (2009)
27. O.G. Kosareva, N.A. Panov, N. Akozbek, V.P. Kandidov, Q. Luo, S.A. Hosseini, W. Liu, J.F. Gravel, G. Roy, S.L. Chin, Appl. Phys. B, Lasers Opt. **82**, 111 (2006)

28. Q. Luo, S.A. Hosseini, W. Liu, J.F. Gravel, O.G. Kosareva, N.A. Panov, N. Akozbek, V.P. Kandidov, G. Roy, S.L. Chin, Appl. Phys. B, Lasers Opt. **80**, 35 (2005)
29. J.F. Daigle, O. Kosareva, N. Panov, M. Bégin, F. Lessard, C. Marceau, Y. Kamali, G. Roy, V. Kandidov, S. Chin, Appl. Phys. B, Lasers Opt. **94**, 249 (2008)
30. S. Skupin, L. Bergé, U. Peschel, F. Lederer, G. Méjean, J. Yu, J. Kasparian, E. Salmon, J.P. Wolf, M. Rodriguez, L. Wöste, R. Bourayou, R. Sauerbrey, Phys. Rev. E **70**, 046602 (2004)
31. M. Mlejnek, M. Kolesik, J.V. Moloney, E.M. Wright, Phys. Rev. Lett. **83**, 2938 (1999)